



HAL
open science

Validation of 4D-flow-based pressure difference estimators

David Nolte, Jesús Urbina, Julio Sotelo, Leo Sok, Cristian Montalba, Israel Valverde, Axel Osses, Sergio Uribe, Cristobal Bertoglio

► To cite this version:

David Nolte, Jesús Urbina, Julio Sotelo, Leo Sok, Cristian Montalba, et al.. Validation of 4D-flow-based pressure difference estimators. 2019. hal-02113750v1

HAL Id: hal-02113750

<https://hal.science/hal-02113750v1>

Preprint submitted on 29 Apr 2019 (v1), last revised 28 Oct 2020 (v3)

HAL is a multi-disciplinary open access archive for the deposit and dissemination of scientific research documents, whether they are published or not. The documents may come from teaching and research institutions in France or abroad, or from public or private research centers.

L'archive ouverte pluridisciplinaire **HAL**, est destinée au dépôt et à la diffusion de documents scientifiques de niveau recherche, publiés ou non, émanant des établissements d'enseignement et de recherche français ou étrangers, des laboratoires publics ou privés.

Validation of 4D-flow-based pressure difference estimators

David Nolte^{1,4}, Jesús Urbina^{2,3}, Julio Sotelo², Leo Sok⁴, Cristian Montalba²
Israel Valverde⁷, Axel Osses^{1,5}, Sergio Uribe^{2,3,5}, Cristóbal Bertoglio^{4,1}

¹Center for Mathematical Modeling, Universidad de Chile

²Biomedical Imaging Center, Pontificia Universidad Católica de Chile

³Department of Radiology, School of Medicine, Pontificia Universidad Católica de Chile

⁴Bernoulli Institute, University of Groningen

⁵Millennium Nucleus for Cardiovascular Magnetic Resonance

⁶Department of Electrical Engineering, Pontificia Universidad Católica de Chile

⁷Hospital Universitario Virgen del Rocío, Sevilla, 41013, Spain

April 29, 2019

Abstract

Purpose: The pressure difference across stenotic blood vessels serves as an important clinical index for the diagnosis of many cardiovascular diseases. While the clinical gold standard for pressure difference measurements is invasive catheterization, Phase-Contrast Magnetic Resonance Imaging is a promising tool for enabling a non-invasive quantification, by linking highly spatially resolved velocity measurements with pressure differences via the incompressible Navier-Stokes equations. In this work we provide a validation with phantom and patient data of pressure difference maps estimators.

Methods: We compare the classical Pressure Poisson Estimator (PPE) and the new Stokes Estimator (STE) against catheter pressure measurements under a large variety of flow regimes. We include several phantom data sets with different anatomic and hemodynamic severities. We also include two patient data sets.

Results: The STE shows always considerably more accuracy than the PPE. Both PPE and STE methods are sensitive to the lumen segmentation, with the STE the less sensitive of both.

Conclusion: The STE appears to be more accurate (compared to catheterization) and more robust to lumen segmentation than the PPE confirming reported findings from numerical experiments.

Keywords: 4D flow, pressure difference, catheter, PPE, STE, validation

1 Introduction

Aortic coarctation (AoCo) is a narrowing of the proximal descending aorta, typically located at the aortic isthmus. AoCo accounts for 5–8% of all congenital heart defects (CHD) and the prevalence of isolated forms is 3 per 10000 live births [14]. The peak-to-peak pressure difference across the coarctation is the most important hemodynamic parameter for clinical decisions [38, 15].

In the clinical practice, different techniques are available to measure pressure differences across aortic coarctations. Catheterization is the gold standard technique, but is expensive, invasive, non-exempt of risk, the patient is exposed to X-rays and is difficult to reproduce. Doppler echocardiography using the simplified Bernoulli equation is the most available non-invasive method, but has certain limitations: it is operator dependent, has poor acoustic windows and spectral broadening, and in addition overestimates the peak velocities up to 25% [18]. Magnetic resonance imaging (MRI) is able to obtain images of the heart and great vessels with an entire coverage of the cardiovascular system for assessment of anatomy, function and flow. Time-resolved three-dimensional phase-contrast MRI (3D cine PC-MRI or 4D Flow MRI) [23, 10] has been proposed to acquire an anatomical image and three velocity encoded images in three orthogonal directions. 4D flow has the capacity to measure non-invasively the 3D-spatial and temporal evolution of complex flow patterns, allowing the quantification of different hemodynamic parameters [24]. In particular, 4D flow allows to create pressure maps using the Navier-Stokes equations along the thoracic aorta.

In order to obtain those maps, the classical method is solving a Pressure Poisson Equation (PPE) by taking the divergence of the Navier-Stokes equations and inserting the velocity measurements in the right-hand-side [13, 19]. More recently, several additional methods have been introduced, a comprehensive review can be found in [3]. In particular, the Stokes Estimator (STE) [36] computes 3D pressure maps using a Stokes equation based on the physical pressure and an auxiliary, non-physical velocity field.

In addition to PPE and STE, less computationally expensive methods exist, like the Work Energy-derived Relative Pressure (WERP) method [9] based on an integral energy balance of the Navier-Stokes equation, the integral momentum relative pressure estimator (IMRP) [3] based on integral linear momentum conservation, or the virtual WERP (vWERP) method [26] based on a different treatment of the convective term than in the IMRP. Using numerical data, the WERP has shown better accuracy than the PPE, but worse accuracy than the STE and IMRP, while the two latter were shown to have similar accuracy [3]. The WERP also assumes that the studied vessel segment does not have bifurcations. As a consequence, it cannot be used to estimate the pressure difference between the ascending and the descending aorta due to the presence of the supra-aortic branches. Moreover, WERP, IMRP and vWERP can only deliver mean pressure differences between two planes of the vessel of interest, and they are therefore difficult to apply in cases when pressure spatial variation are present as in post stenotic areas. For all the aforementioned reasons, in this work we consider only the PPE and the STE methods.

To the best of the authors' knowledge, no validation studies have been reported for the STE method using real 4D flow and catheterization data. Several validation studies

were carried out for the PPE method [30, 31, 16]. An in vitro validation study showed a good correlation between PPE and catheter pressure differences ($r = 0.89$, $p < 0.001$) in the simple setting of an elastic straight tube phantom [30]. The PPE method was further assessed in 13 patients with moderate AoCo in [31], where instantaneous peak pressure differences from 4D flow were found to be slightly underestimated on average in comparison to the catheterization data, with a bias of 1.5 mmHg and a variability of ± 4.6 mmHg (two standard deviations). Also in [16], PPE pressure differences showed good agreement with catheter measurements in AoCo patients in cases with sufficient spatial image resolution (at least 5 voxels/diameter). However, systematic underestimation of the pressure difference was found for lower resolutions (3.4 ± 0.64 voxels/diameter).

Performing a sensitivity study of pressure difference estimation methods from 4D flow in patients with cardiovascular diseases under different physiological conditions, i.e. under rest and stress, is challenging. First, the length of the scan time for acquiring 4D flow data limits the number of scans that can be acquired in patients, i.e., under different physiological conditions. Also, it is difficult to obtain serial images to evaluate the natural evolution of the aortic coarctation. Secondly, it is difficult to build a robust analysis of the results due to the complex interaction between many physiological variables controlled by hormonal, mechanical and chemistry signals. Finally, it is difficult and risky to expose coarctation patients to different conditions of stress and cardiac load.

To circumvent these limitations, vessel phantom studies have been used in controlled experiments to visualize flow patterns and validate physiological measurements obtained from 2D and 4D flow in order to improve the understanding of CVD [22, 35, 6, 39]. Recently, we have designed and studied a MRI compatible aortic phantom simulating normal and AoCo conditions and compared its hemodynamics with healthy volunteers and AoCo patients [37].

The aim of this work is to study the effects of the MR image resolution and aortic segmentation, cardiac output and severity of the aortic coarctation on the accuracy of pressure difference reconstruction methods from 4D flow velocity data using a realistic aortic coarctation phantom. We compare the performance of the PPE and the STE methods under these aspects with pressure gradients obtained by catheterization. To the best of the authors' knowledge, the present study is the first reported validation of the STE method using real data.

Both relative pressure reconstruction methods were also applied to and compared for two patients with aortic coarctation for whom combined 4D flow and catheterization was performed.

2 Theory

Maps of relative pressure can be computed directly from the velocity measurements by evaluating the linear momentum conservation equation of the incompressible Navier–Stokes model, i.e.

$$-\nabla p = \rho \frac{\partial \vec{u}}{\partial t} + \rho(\vec{u} \cdot \nabla)\vec{u} - \mu \Delta \vec{u} \quad (1)$$

where ρ is the density of the fluid and μ its dynamic viscosity, $\vec{u} : \Omega \rightarrow \mathbb{R}^3$ denotes the velocity vector field and $p : \Omega \rightarrow \mathbb{R}$ is the pressure field. Ω represents the computational domain obtained from segmenting the 4D flow images. By inserting the 4D flow velocity data into \vec{u} , the pressure gradient can be recovered by applying numerical methods. In this work we use the Poisson Pressure Equation (PPE) approach [13, 12, 19] and the Stokes Estimator method (STE) [36, 8], which will be described in this section.

Discretizing Equation (1) in time, here with the first order backward difference formula, gives the following expression for the pressure gradient:

$$-\nabla p^k = \rho \frac{\vec{u}^k - \vec{u}^{k-1}}{\Delta t} + \rho(\vec{u}^k \cdot \nabla)\vec{u}^k - \mu\Delta\vec{u}^k. \quad (2)$$

The indices $1 \leq k \leq N$ denote the time snapshot of the measurements and Δt the temporal offset between two consecutive measurements or cardiac phases, with time stamps $t_k = k\Delta t$. For the first step, $k = 1$, a forward difference has to be used instead since no previous measurements are available. Evaluating the right hand side of Equation (2) for spatially undersampled and noisy velocity measurements \vec{u}_m ,

$$R^k := \rho \frac{\vec{u}_m^k - \vec{u}_m^{k-1}}{\Delta t} + \rho(\vec{u}_m^k \cdot \nabla)\vec{u}_m^k - \mu\Delta\vec{u}_m^k. \quad (3)$$

yields a pressure gradient estimate $\nabla \hat{p}^k \approx \nabla p^k$, given by

$$-\nabla \hat{p}^k = R^k. \quad (4)$$

Higher order time schemes, while more accurate in theory for small time steps, are not beneficial in the present context due to the coarse time sampling of the measured velocities. Note that in previous works, for instance in [3, 26] a second-order mid-point scheme was used. However, this leads to stronger underestimations of the pressure differences. This can be explained from the nature of time under-sampling in MRI, namely that u_m^k is reconstructed by assuming the flow velocity as constant within the interval $[t^k - \Delta t/2, t^k + \Delta t/2]$ rather than being an instantaneous measurement at t^k [25].

It is important to remark that in all methods derived from the Navier-Stokes equations, e.g., Bernoulli-based, PPE, STE, and in CFD simulations, at any instant of time, the pressure is uniquely defined up to a constant (with respect to the spatial coordinates). Therefore, only instantaneous pressure differences between different locations can be compared at different times. Catheterization or sphygmomanometer pressure measurements are taken relative to the atmospheric pressure. Hence, the pressures are calibrated with respect to a global reference and pressure values can be compared at different times and among patients. A common measure in the clinical practice are the so-called peak-to-peak pressure differences, which compares the largest pressure difference registered between two locations at any time during the cardiac cycle, thus taking into account time shifts due to the vessel elasticity. Peak-to-peak pressure differences can only be determined by means of catheterization or with the models described above when calibrated with catheterization data, which however

violates the non-invasiveness of the estimation methods. For this reason, the present work focuses on instantaneous pressure differences instead of peak-to-peak values.

Based on Equation (4), the Pressure Poisson Equation (PPE) and the Stokes Estimator (STE) method will be described next.

2.1 Poisson pressure equation (PPE)

Assuming sufficient regularity (i.e., assuming that all required derivatives exist), a Poisson equation for the pressure estimation can be obtained by taking the divergence of the time-discrete Navier–Stokes equation (2),

$$-\Delta \hat{p}^k = \nabla \cdot R^k. \quad (5)$$

Solving Equation (5) requires boundary conditions (BCs) on the boundary $\partial\Omega$ of the computational domain. A priori, no physical BCs for the pressure are known. An artificial Neumann BC can be obtained by projection of Equation (4), restricted to $\partial\Omega$, to the outward unit normal vector on the wall, \vec{n} ,

$$\vec{n} \cdot \nabla \hat{p}^k = \vec{n} \cdot R^k. \quad (6)$$

Equation (5) with BCs (6) can be discretized in space and solved with the finite element, finite volume or finite difference methods. Independently on the spatial discretization, in order to ensure that the resulting algebraic problem is uniquely solvable, an option is to fix $\hat{p}^k = 0$ at one point via a Dirichlet boundary condition. This, indeed, does not change the pressure differences between two points in space.

2.2 Stokes Estimator (STE)

The Stokes Estimator introduces a divergence-free auxiliary function \vec{w} with $\vec{w} = \vec{0}$ on $\partial\Omega$. The Laplacian of \vec{w} is subtracted from Equation (4) as a regularization term (with unitary viscosity here for simplicity) and we obtain

$$\begin{aligned} -\Delta \vec{w} - \nabla \hat{p}^k &= R^k & \text{in } \Omega \\ \nabla \cdot \vec{w} &= 0 & \text{in } \Omega \\ \vec{w} &= \vec{0} & \text{on } \partial\Omega. \end{aligned} \quad (7)$$

The auxiliary function \vec{w} holds no physical interest, and it is expected to be negligible compared to the pressure term as long as the right-hand-side R^k is the gradient of a scalar (irrotational). The advantages with respect to the PPE method are (1) that no artificial BCs for the pressure are necessary and (2) lower regularity requirements, since no additional derivatives are applied on the measurements R^k . In fact, in contrast to the PPE method, the STE method searches the pressure in the natural energy space of the pressure in the original Navier–Stokes equations. As for the PPE method, the pressure constant has to be fixed for ensuring solvability of the algebraic problem.

A variation of the STE method was presented in [3], where the convective term was written in ‘energy-conserving’ form, $(\vec{u} \cdot \nabla)\vec{u} + \frac{1}{2}(\nabla \cdot \vec{u})\vec{u}$, and improved results were obtained compared to the standard method. A third way of formulating the convection term is the divergence form $\nabla \cdot (\vec{u} \otimes \vec{u})$. In a preliminary study, the standard method, Eq. (3) (results not shown here), consistently delivered more accurate results than the other variants. Hence only results obtained using the standard STE formulation will be reported here.

3 Methods

3.1 Aortic Phantom Study

3.1.1 Phantom setup

The aortic phantom is fully described in [37] and [27]. Different degrees of aortic coarctation were placed in the descending aorta just after the left subclavian artery. Aortic coarctations were built with Technyl with an effective orifice of 13, 11 and 9 mm and a length of 10 mm, leading to coarctation indices of 0.6, 0.5 and 0.4 respectively. The coarctation index was defined as the ratio between the AoCo diameter and the diameter of the native DAo distal to the AoCo. The liquid used in the system consisted of a blood mimicking fluid homemade with 60 % distilled water and 40 % glycerol (Orica Chemicals, Watkins, CO), with a density of 1.119 g/cm^3 , viscosity of $4.83 \times 10^{-3} \text{ Pa}\cdot\text{s}$, and a T1 value of 900 ms, which are representative values for human blood.

3.1.2 Catheterization

The phantom was equipped with a catheterization unit to measure invasively and simultaneously the pressure gradient across the coarctation. For this purpose, two catheters (5 French, Soft-Vu, AngioDynamics, Latham, NY) with transducers (AngioDynamics) were placed in the AAo and 2 cm after the AoCo and were connected to a patient monitor (Contec Medical Systems, Hebei, China). The pressure catheters were zeroed at the same height of the phantom.

Pressure information from the two catheters was recorded simultaneously during 1 minute in the AoCo phantoms (9 mm, 11 mm, 13 mm) at rest (75 bpm) and at stress conditions (136 bpm), using the commercial software Central Monitor System V3.0 (Contec Medical System). The pressure difference is obtained by subtracting both time series and averaging over the cardiac cycles.

3.1.3 4D flow data acquisition

Phantom data were acquired in a 1.5 T MRI system (Achieva, Philips, The Netherlands) using a 4-channel body coil and retrospective cardiac gating. The control unit of the pulsatile pump generated a trigger signal to synchronize the MR data acquisition. In order to provide

Table 1: MR acquisition parameters

	in-vitro experiments	in-vivo experiments
FOV (mm)	$200 \times 200 \times 114$	$270 \times 270 \times 125$
Matrix size	$224 \times 224 \times 127$	$144 \times 144 \times 50$
Recon. voxel (mm)	$0.9 \times 0.9 \times 0.9$	$1.9 \times 1.9 \times 2.5$
TFE factor	rest: 2, stress: 1	rest: 2
Cardiac phases	25	28
Time resolution (ms)	AoCo: rest: 32, stress: 18 Normal: rest: 35, stress: 19	rest: 26
VENC (cm/s)	AoCo: rest: 160–400, stress: 250–500 Normal: rest: 150, stress: 150	rest: 300
TE/TR (ms)	3.7/6.4	2.4/3.8
Flip angle (deg)	6.5	5
Scan time (min)	18–22	19

static tissue for phase correction algorithms used in PC-MRI, 6 liters of 1% agar were placed around the aortic phantom at least 6 hours before scanning.

4D flow images were acquired with an isotropic voxel size of 0.9 mm for all phantoms (AoCo with 9 mm, 11 mm and 13 mm orifice diameter) under rest and stress conditions. The acquisition parameters are summarized in Table 1 (see column “in-vitro experiments”).

In order to study the effect of image resolution of the pressure gradient estimation procedure, different synthetic low resolution data (1.4 and 2.0 mm isotropic voxel) were generated from the original image (0.9 mm isotropic voxel) using linear interpolation.

3.2 Patient study: 4D-Flow MRI and catheterization

In addition to the phantom study, we include two subjects with aortic coarctation (Subject 1: 12 years, weight 47 kg, height 151 cm; Subject 2: 35 years, weight 63 kg, height 205 cm), who underwent combined MRI (4D Flow MRI) and cardiac catheterization investigations, in a 1.5T Achieva MR scanner and a BT Pulsera cardiac radiography unit (Philips, Best, Netherlands). The data was acquired at St. Thomas’ Hospital, London, UK. The local research ethics committee approved this retrospective study and informed consent was obtained from all patients. Subject 1 presented a native aortic coarctation and mild aortic valve stenosis, mild left ventricular hypertrophy and systemic hypertension at rest. Subject 2 presented a repaired AoCo using a subclavian flap, situs solitus, there was a very mild narrowing at the level of the transverse arch, close to the isthmus and a mild dilatation in the proximal descending aorta and also presented a gothic aortic arch. The acquisition parameters for the in vivo study are summarized in Table 1 (see column “in vivo experiments”).

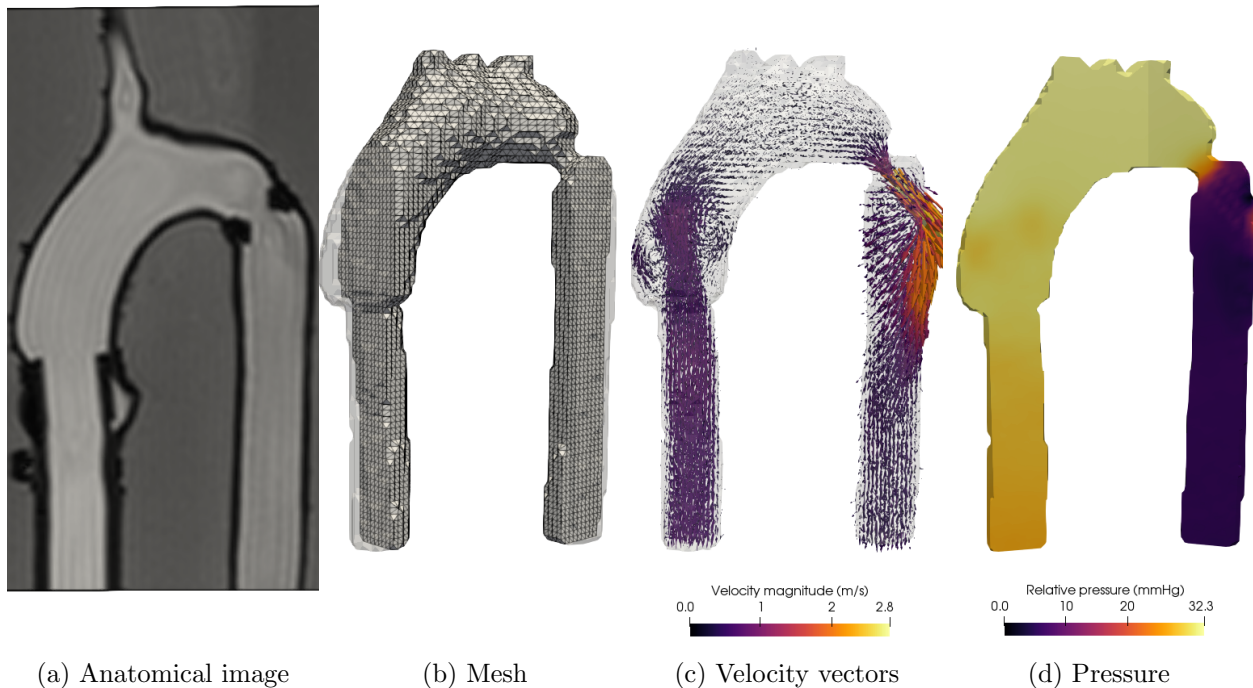


Figure 1: Pressure recovery toolchain. (a) 2D section from the anatomic image of 4D Flow MRI, (b) structured tetrahedral mesh from segmentation of the anatomical image, (c) representation of 4D flow velocity vectors on mesh, (d) pressure maps from velocity data (cuts through centers of AAo and DAo). Example data of the 9 mm AoCo phantom at rest, at time of peak systole.

3.3 Segmentation and mesh generation

The 4D Flow MRI data sets were processed using an in-house MATLAB library (The MathWorks, Natick, MA), similarly to previous studies [34, 33]. This process is illustrated in Figure 1 and consisted of the segmentation of the thoracic aorta using the anatomical image (Figure 1(a)) for the phantom data or the angiographic image proposed in [4] for patients. The value of the threshold is around 20% of the maximum intensity of the image. After applying the threshold, we manually clean the vessel of interest, using labeling and manual delimitation tools of MATLAB. From the final segmented image, we generated a structured tetrahedral mesh (Figure 1(b)) such that its vertices matched the centers of the image voxels. Once the mesh was constructed, each velocity vector was transferred from the 4D flow MRI data to each node of the mesh (Figure 1(c)). The last step in the toolchain consists in the pressure map reconstruction (Figure 1(d)), described in the next section.

In order to study the effect of different segmentations on the pressure difference estimates, additional segmentations were created for the phantom velocity images at 0.9 mm voxel size. A reference segmentation was modified by adding or subtracting one voxel at the boundary,

thus extending or decreasing the lumen cross-section.

A preliminary study compared our structured meshing approach to generic tetrahedral meshes and found a significantly improved accuracy of the pressure estimation methods at similar mesh sizes. Here, only the results obtained with structured meshes are considered.

3.4 Pressure maps computation

Pressure maps are computed from all 4D flow data sets with the PPE and STE methods. The pressure differences, to be compared with the corresponding catheter values, are defined as differences of the pressure averages over two spheres with a radius of 4 mm at locations proximally and distally to the AoCo (e.g., the blue and red spheres in Figure 2).

The corresponding partial differential equations of the PPE and STE methods are discretized with the finite element method (FEM). Velocity measurements are assumed to be piece-wise linear (\mathbb{P}^1) finite element functions on the tetrahedral meshes described in the previous section. Linear \mathbb{P}^1 elements are also used to discretize the PPE and the STE systems, Equations (5) and (7). In the latter case, standard pressure stabilization (Brezzi-Pitkaranta) is employed to ensure the solvability of the saddlepoint problem, avoiding the need of higher order elements. A sample pressure map computation is shown in Figure 1(d), as result of the last step of the pressure recovery toolchain, described in the previous section and illustrated in Figures 1(a)-(d). The code was implemented using the python/C++ FEM library FEniCS [1] and linear algebra solvers from the scientific computation library PETSc [2]. The computation times are compared in Table 2.

Table 2: Computation times and numbers of unknowns of the 13 mm phantom at different resolutions with the PPE and the STE methods using 1 or 4 cores of an Intel Xeon E5-1620 CPU. With the highest resolution of 0.9 mm, iterative solvers have to be used for the STE method due to memory requirements (on a 32GB RAM workstation). We employed the GMRES method [32] with a Schur complement based block preconditioner, using algebraic multigrid on the ‘velocity’ block and the diagonal of a pressure mass matrix for the Schur complement.

# CPUs	resolution	PPE		STE	
		# unknowns	time	# unknowns	time
1	2 mm	19597	5.2 s	78388	29.1 s
4	0.9 mm	240519	13.7 s	962076	702.0 s

4 Results

4.1 Phantom study

The streamlines of the 4D flow velocity field and the pressures measured by catheterization in the indicated locations are illustrated in Figure 2 for the 9 mm AoCo phantom at peak

systole. In addition, the instantaneous pressure difference resulting from subtracting both signals is plotted.

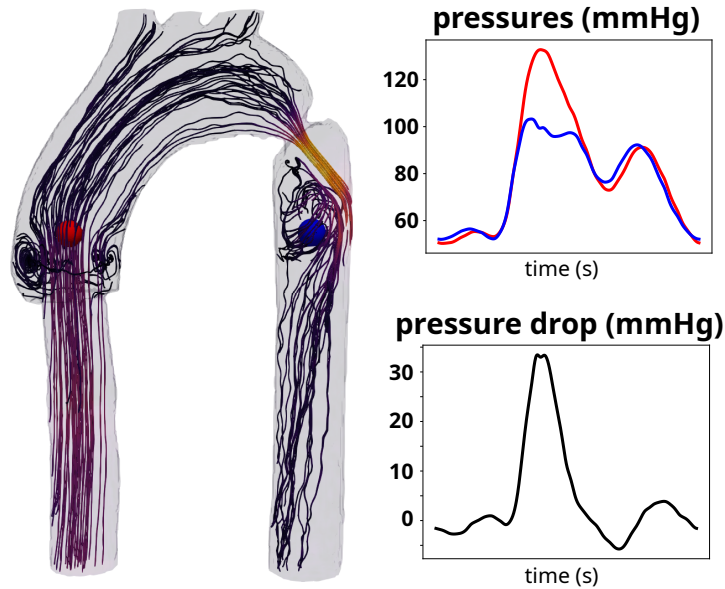


Figure 2: 9 mm phantom at rest. Velocity streamlines at peak systole, catheterization pressure signals, measured at blue and red dots, and resulting pressure differences.

Figure 3 compares the instantaneous peak pressure differences obtained with the PPE and the STE methods from 4D flow with catheterization data for all investigated phantoms. The figure shows the data obtained with the three image resolutions, 0.9 mm, 1.4 mm and 2.0 mm and using the three segmentations, denoted V+0 (neutral), V-1 (outermost layer of voxels eliminated along the boundary) and V+1 (1 layer of voxels added at the boundary).

Consider first the results obtained on the V+0 segmentation. The results show an overall good agreement between the STE peak pressure differences and the catheterization data. The STE underestimates the highest measured pressure difference (catheter pressure difference of 46 mmHg with the 9 mm AoCo phantom under stress conditions). Another underestimation is visible at 12 mmHg in all plots, which was obtained for the 13 mm phantom at rest. The results appear to be robust to the image resolution. A strong dependence on the segmentation exists particularly for pressure differences above 30 mmHg and is more pronounced for large voxel sizes. The PPE method, in comparison, leads to a stronger underestimation than the STE method for pressure differences ≥ 20 mmHg. The PPE results are more sensitive to the image resolution.

In the presence of large pressure differences, both the PPE method and the STE method generally benefit from the narrowed segmentation (denoted V-1 in the figure). In the range of moderate pressure differences (e.g., 10–20 mmHg), the most accurate results with the STE method were obtained on the reference segmentation, while the V-1 segmentation led to a slight overestimation. The accuracy of the PPE method however was improved throughout the entire range of pressure differences. This is likely because of an increased sensitivity to

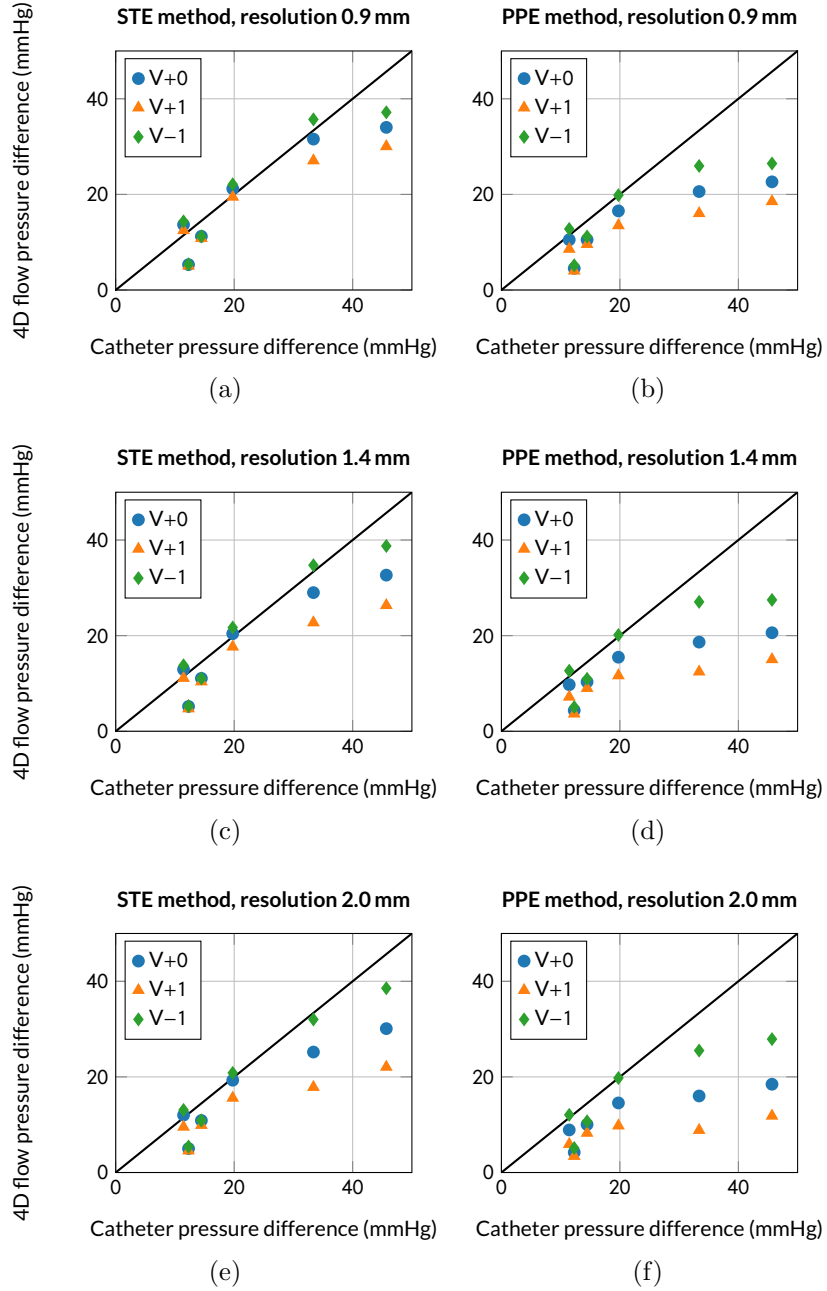


Figure 3: Comparison of 4D flow peak pressure differences obtained with the STE (left column) and the PPE (right column) methods with catheterization. Figures (a) and (b) show results obtained using an image resolution of 0.9 mm, (c) and (b) a resolution of 1.4 mm, and (e) and (f) a resolution of 2 mm. V+0 refers to a reference segmentation, V+1 denotes results obtained using V+0 extended by 1 voxel in each direction along the wall, and V-1 is the segmentation V+0 with the outer layer of voxels deleted.

boundary issues such as partial volume effects and low VNR (velocity-to-noise ratio) due to the artificial pressure boundary conditions. Choosing the segmentation too large resulted in underestimating the pressure differences (V+1 values in Figure 3).

The mean signed difference, as a measure of the bias, and the spread (two standard deviations) of the PPE and the STE methods with respect to catheterization data are compared for the three segmentations, V+0, V-1 and V+1 in Table 3. The data is shown for the acquired 4D flow images with a resolution of 0.9 mm. The bias and variability are

Table 3: Mean signed difference (bias) \pm spread (two standard deviations) for the PPE and the STE methods with respect to catheterization data, for the standard (V+0), the reduced lumen diameter segmentation (V-1), and the widened lumen diameter segmentation (V+1). 4D flow resolution: 0.9 mm

<u>method</u>	V+0	V-1	V+1
	bias $\pm 2\sigma$	bias $\pm 2\sigma$	bias $\pm 2\sigma$
PPE	-8.62 \pm 14.97 mmHg	-5.94 \pm 13.56 mmHg	-11.13 \pm 17.01 mmHg
STE	-3.34 \pm 9.61 mmHg	-1.85 \pm 9.29 mmHg	-5.35 \pm 10.94 mmHg

smallest on the reduced segmentation V-1 and largest on the extended segmentation V+1, with the reference segmentation V+0 ranking in between. The PPE method appears to be more sensitive to the segmentation. The STE method gives a smaller bias and variability than the PPE method on all segmentations. In particular, the STE result on the standard V+0 segmentation appears to be more accurate than the PPE result obtained on the V-1 segmentation.

Time profiles of the pressure differences obtained with the V-1 segmentation are shown in Figures 4-6. Each figure contains the results of the PPE and the STE methods for 4D flow image resolutions of 0.9 mm (acquired) and 1.4 mm, 2.0 mm (subsampling from 0.9 mm) under rest and stress conditions and the pressure difference from catheter measurements.

The results of the 13 mm AoCo phantom study are displayed in Figure 4. While showing qualitatively a correct behavior, the amplitude of the oscillation is generally underestimated by 3 to 7 mmHg with both methods under rest conditions. The effect of the image resolution is hardly noticeable (although slightly larger with the PPE method). Under stress conditions, the peak pressure difference is recovered with a good accuracy. There is a negative pressure difference peak that was not correctly recovered by any of both methods. It has to be noted that in the particular case of the 13 mm AoCo phantom, artifacts appeared in the velocity measurements, most likely connected to issues with the experimental setup, like bubbles. The 13 mm AoCo phantom configuration was repeatedly scanned at different resolutions (results not reported) and the corresponding estimated pressure differences showed similar characteristics in all cases.

In the case of the 11 mm AoCo phantom, the PPE method exhibits a very good quantitative agreement with the catheter results under rest conditions during the complete heart cycle

(Figure 5(b)). In comparison, the STE method overestimates the peak pressure difference. The STE result is improved by using the standard segmentation instead of the narrowed segmentation. Under stress conditions, the width of the pressure differences maxima was overestimated with both the STE and the PPE methods.

Results from the 9mm AoCo phantom under rest conditions showed an excellent agreement between the catheter data and the pressure difference computed with the STE method (Figure 6, panel (a)). The PPE method strongly underestimates the pressure difference under equal conditions (panel (b)). The discrepancy between the pressure difference reconstruction and catheter measurements increases for stress conditions, the STE method still showing more accurate results than the PPE method. Both methods are very robust with respect to the image resolution. Using the narrowed segmentation, the results of the stress case are slightly improved by the lower resolutions. With low resolution data, effectively more boundary data is discarded by deleting the outermost voxel layer. This indicates that the errors introduced by considering boundary data predominate the effect of image resolution in this scenario. In contrast, in Figure 3 the V+0 pressure differences at 46 mmHg decrease with lower image resolutions.

4.2 Patient data

Pressure differences obtained by catheterization and from 4D flow are shown in Figure 7 for both patients. The pressure difference computed with the STE method for subject 1 shows excellent agreement with the catheter data during systole, underestimating the local extrema after $t = 0.4$ s. While similar qualitative agreement was found with the PPE method, it significantly underestimates the pressure difference during systole. Subject 2 exhibits excellent qualitative and quantitative agreement between catheter data and numerical pressure difference reconstruction. However, the pressure difference peak observed by catheterization is too steep to be captured by the time resolution of the 4D flow protocol. The resulting maximum value lies below the catheter value, possibly because no velocity image was recorded coinciding exactly with the maximum pressure difference.

Note that the lengths of the cardiac cycles differ significantly between catheterization and MRI scans of both patients. This indicates a change in the heart rate and hence, the hemodynamics in the cardiovascular system, and can explain the differences between 4D flow and catheter pressure differences.

Reducing the diameter of the segmentation by one voxel was not possible in one of the patients due to the large voxel size with respect to the diameter. The original segmentations were thus not modified.

5 Discussion

This study compared two relative pressure reconstruction methods, STE and PPE, in terms of accuracy and sensitivity with respect to image resolution, segmentation, AoCo severity and cardiac load (rest and stress). The main finding of this study is that the STE method

applied to real data is more accurate than the classical PPE method at large pressure differences (>20 mmHg). The difference between the methods is less pronounced for small to moderate pressure gradients. The PPE method showed overall a higher sensitivity to data perturbations, i.e., to image resolution and segmentation. Both the STE and the PPE methods proved most sensitive to the image resolution and the segmentation in the most severe cases of 9 mm and 11 mm AoCo during systole. Especially the PPE results were greatly improved by eliminating the outermost layer of voxels from the segmentation, leading to a more accurate match with the catheter data than STE in the 11 mm AoCo phantom. However, the STE method gave excellent results in this case using the standard segmentation. A reduction of the segmentation was used before in [16] and also led to an improved accuracy of the PPE method. The accuracy improvement can be explained by the reduction of partial volume effects and eliminating low VNR data near the boundaries. The PPE method is likely to be more sensitive to the boundary data than the STE method due to the artificial pressure boundary conditions used in the PPE. The issues of boundary data, possible remedies and the effect of somewhat arbitrarily reducing the diameter of the vessel geometry deserve a more in-depth analysis in future studies.

Our results on the standard segmentation (V+0) are coherent with [28, 16], who also demonstrated that the pressure profile is degraded when the spatial resolution is decreased. In [16], minimal resolution requirements were determined for the PPE, namely 5 voxels/diameter. In our study, when the narrowed segmentation was used (V−1, between 2 and 12 voxels/diameter for the AoCo phantoms), the results were almost insensitive to the image resolution. It is possible that the benefit of removing problematic boundary data at low resolutions, apparently increasing under low resolutions, balances with the detriment of a decreased image resolution in the interior.

An advantage of the STE method is that it avoids unphysical boundary conditions. However, using standard discretization methods, parts of the term R^k in Equation (7) can contribute to the auxiliary function—not always negligible in practice—instead of the pressure gradient. This occurs principally where large gradients are present in the velocity field, for instance in the coarctation near the arterial walls, and can result in stronger underestimations of the relative pressure. We hypothesize that, by choosing a more narrow segmentation with the arterial wall located inside the flow, the homogeneous Dirichlet boundary condition for the auxiliary velocity in the STE on the smaller domain results in a smaller auxiliary velocity everywhere and therefore in increased pressure gradient estimates with respect to the full geometry for severe AoCo. Pressure-robust FEM could counteract this issue [21] and generally improve the accuracy of the STE method.

Dilated segmentations (V+1) add no-flow voxels with very small VNR, hence introducing spurious information into the estimation problem. The pressure gradient computed with any method is required to accommodate to the unphysical conditions.

For severe conditions of AoCo, i.e., in the presence of high velocity jets and high Reynolds numbers, the STE method was clearly superior to the PPE method. In such severe cases of AoCo, turbulence can develop [20, 11] and involves dynamics at scales smaller than the spatial and/or temporal image resolution. Such effects are not accounted for by the models

studied here, and are likely to reduce the precision especially in the 9 mm phantom under stress conditions. Furthermore, higher velocities require higher VENC values (500 cm/s for the 9 mm phantom at stress) resulting in lower VNR, possibly affecting the estimation. Our study did not include sensitivity to noise. However, we can consider the results present here as a “worst case scenario” in terms of noise due to the small voxel size of 0.9 mm, hence involving a much worse VNR than what can be expected for typical voxel size in patients (i.e., around 2 mm). This issue could be alleviated by using the dual-VENC techniques [29, 17, 5, 7], allowing for lower VENC-values (hence lower noise), but at increased scan times.

The STE and the PPE pressure reconstruction methods were also applied to real patient data. For one of the patients, the STE method showed a great improvement over the PPE method. Both methods showed satisfactory results for the second patient. From the findings in the phantom experiments, the differences between PPE and STE in patient one is most likely due to strong convective effects.

One limitation of the study was the lack of availability of real low resolution MRI data for all scenarios, hence requiring synthetic subsampling of the high resolution data. In addition, the comparison of catheter data with MRI scans is limited by the following observations. The locations where the catheter recorded the pressure during catheterization are only known approximately. Fluctuations in the flow can also perturb the catheter position. A mismatch of the catheter positions with the locations selected for evaluating the computed pressure gradient can introduce additional errors. Finally, representing an invasive technique, it is possible that the presence of the catheter in the vessel disturbs and alters the aortic flow during catheterization, while the 4D flow data was acquired immediately after without the catheters. In the patient study it was seen that the heart rate changed significantly between catheterization and the MRI scan, hence possibly also affecting the outcome of this comparison.

In conclusion, in our phantom study, the STE method delivered results that were more accurate and robust with respect to resolution and segmentation than the PPE method, in particular in severe cases of AoCo. For cases of mild AoCo or no AoCo, the advantage of the STE method was negligible. By eliminating the outermost layer of voxels of the segmentation, the PPE method could be significantly improved to match the accuracy of the STE method, except for very large pressure gradients.

conflict of interest

The authors declare no conflict of interest.

References

- [1] Martin Alnæs, Jan Blechta, Johan Hake, August Johansson, Benjamin Kehlet, Anders Logg, Chris Richardson, Johannes Ring, Marie E. Rognes, and Garth N. Wells. The

FEniCS Project Version 1.5. Archive of Numerical Software, 3(100), 2015.

- [2] Satish Balay, Shrirang Abhyankar, Mark F. Adams, Jed Brown, Peter Brune, Kris Buschelman, Lisandro Dalcin, Alp Dener, Victor Eijkhout, William D. Gropp, Dinesh Kaushik, Matthew G. Knepley, Dave A. May, Lois Curfman McInnes, Richard Tran Mills, Todd Munson, Karl Rupp, Patrick Sanan, Barry F. Smith, Stefano Zampini, Hong Zhang, and Hong Zhang. PETSc Users Manual. Technical Report ANL-95/11 - Revision 3.10, Argonne National Laboratory, 2018.
- [3] Cristóbal Bertoglio, Rodolfo Nuñez, Felipe Galarce, David Nordsletten, and Axel Osses. Relative pressure estimation from velocity measurements in blood flows: State-of-the-art and new approaches: Relative pressure estimation. International Journal for Numerical Methods in Biomedical Engineering, 34(2):e2925, February 2018.
- [4] Jelena Bock, Alex Frydrychowicz, Aurélien F. Stalder, Thorsten A. Bley, Hans Burkhardt, Jürgen Hennig, and Michael Markl. 4D phase contrast MRI at 3 T: Effect of standard and blood-pool contrast agents on SNR, PC-MRA, and blood flow visualization. Magnetic Resonance in Medicine: An Official Journal of the International Society for Magnetic Resonance in Medicine, 63(2):330–338, 2010.
- [5] Fraser Callaghan, Rebecca Kozor, Andrew Sherrah, Michael Vallely, David Celermajer, Gemma Figtree, and Stuart Grieve. Use of multi-velocity encoding 4d flow mri to improve quantification of flow patterns in the aorta. Journal of Magnetic Resonance Imaging, 43(2):352–363, 2016.
- [6] C. Canstein, P. Cachot, A. Faust, A. F. Stalder, J. Bock, A. Frydrychowicz, J. Küffer, J. Hennig, and Michael Markl. 3D MR flow analysis in realistic rapid-prototyping model systems of the thoracic aorta: Comparison with in vivo data and computational fluid dynamics in identical vessel geometries. Magnetic Resonance in Medicine: An Official Journal of the International Society for Magnetic Resonance in Medicine, 59(3):535–546, 2008.
- [7] Hugo Carrillo, Axel Osses, Sergio Uribe, and Cristóbal Bertoglio. Optimal Dual-VENC (ODV) Unwrapping in Phase-Contrast MRI. IEEE transactions on medical imaging, 2018.
- [8] M. E. Cayco and R. A. Nicolaides. Finite element technique for optimal pressure recovery from stream function formulation of viscous flows. Mathematics of computation, 46(174):371–377, 1986.
- [9] Fabrizio Donati, C. Alberto Figueroa, Nicolas P. Smith, Pablo Lamata, and David A. Nordsletten. Non-invasive pressure difference estimation from PC-MRI using the work-energy equation. Medical image analysis, 26(1):159–172, 2015.
- [10] Petter Dyverfeldt, Malenka Bissell, Alex J. Barker, Ann F. Bolger, Carl-Johan Carlhäll, Tino Ebbers, Christopher J. Francios, Alex Frydrychowicz, Julia Geiger, Daniel Giese,

- Michael D. Hope, Philip J. Kilner, Sebastian Kozerke, Saul Myerson, Stefan Neubauer, Oliver Wieben, and Michael Markl. 4D flow cardiovascular magnetic resonance consensus statement. Journal of Cardiovascular Magnetic Resonance, 17(1), December 2015.
- [11] Petter Dyverfeldt, Andreas Sigfridsson, John-Peder Escobar Kvitting, and Tino Ebbers. Quantification of intravoxel velocity standard deviation and turbulence intensity by generalizing phase-contrast MRI. Magnetic Resonance in Medicine, 56(4):850–858, October 2006.
- [12] Tino Ebbers and Gunnar Farneböck. Improving computation of cardiovascular relative pressure fields from velocity MRI. Journal of Magnetic Resonance Imaging, 30(1):54–61, 2009.
- [13] Tino Ebbers, L. Wigstrom, A. F. Bolger, Bengt Wranne, and Matts Karlsson. Noninvasive measurement of time-varying three-dimensional relative pressure fields within the human heart. Journal of biomechanical engineering, 124(3):288–293, 2002.
- [14] Raimund Erbel, Victor Aboyans, Catherine Boileau, Eduardo Bossone, Roberto Di Bartolomeo, Holger Eggebrecht, Arturo Evangelista, Volkmar Falk, and Herbert Frank. 2014 ESC Guidelines on the diagnosis and treatment of aortic diseases: Document covering acute and chronic aortic diseases of the thoracic and abdominal aorta of the adult. The Task Force for the Diagnosis and Treatment of Aortic Diseases of the European Society of Cardiology (ESC). European heart journal, 35(41):2873–2926, 2014.
- [15] Timothy F. Feltes, Emile Bacha, Robert H. Beekman III, John P. Cheatham, Jeffrey A. Feinstein, Antoinette S. Gomes, Ziyad M. Hijazi, Frank F. Ing, Michael De Moor, and W. Robert Morrow. Indications for cardiac catheterization and intervention in pediatric cardiac disease: A scientific statement from the American Heart Association. Circulation, 123(22):2607–2652, 2011.
- [16] Leonid Goubergrits, Florian Hellmeier, Dominik Neumann, Viorel Mihalef, Mehmet A. Gulsun, Marcello Chinali, Aurelio Secinaro, Kilian Runte, Stephan Schubert, Felix Berger, Titus Kuehne, Anja Hennemuth, and Marcus Kelm. Patient-specific requirements and clinical validation of MRI-based pressure mapping: A two-center study in patients with aortic coarctation. Journal of Magnetic Resonance Imaging, 49(1):81–89, 2019.
- [17] Hojin Ha, Guk Bae Kim, Jihoon Kweon, Young-Hak Kim, Namkug Kim, Dong Hyun Yang, and Sang Joon Lee. Multi-vec acquisition of four-dimensional phase-contrast mri to improve precision of velocity field measurement. Magnetic resonance in medicine, 75(5):1909–1919, 2016.
- [18] P. R. Hoskins. Accuracy of maximum velocity estimates made using Doppler ultrasound systems. The British journal of radiology, 69(818):172–177, 1996.

- [19] Sebastian B. S. Krittian, Pablo Lamata, Christian Michler, David A. Nordsletten, Jelena Bock, Chris P. Bradley, Alex Pitcher, Philip J. Kilner, Michael Markl, and Nic P. Smith. A finite-element approach to the direct computation of relative cardiovascular pressure from time-resolved MR velocity data. Medical Image Analysis, 16(5):1029–1037, July 2012.
- [20] David N. Ku. Blood flow in arteries. Annual review of fluid mechanics, 29(1):399–434, 1997.
- [21] A. Linke and C. Merdon. Pressure-robustness and discrete Helmholtz projectors in mixed finite element methods for the incompressible Navier–Stokes equations. Computer Methods in Applied Mechanics and Engineering, 311:304–326, November 2016.
- [22] R. Lorenz, C. Benk, J. Bock, A. F. Stalder, J. G. Korvink, J. Hennig, and M. Markl. Closed circuit MR compatible pulsatile pump system using a ventricular assist device and pressure control unit. Magnetic resonance in medicine, 67(1):258–268, 2012.
- [23] Michael Markl, Francis P. Chan, Marcus T. Alley, Kris L. Wedding, Mary T. Draney, Chris J. Elkins, David W. Parker, Ryan Wicker, Charles A. Taylor, and Robert J. Herfkens. Time-resolved three-dimensional phase-contrast MRI. Journal of Magnetic Resonance Imaging: An Official Journal of the International Society for Magnetic Resonance in Medicine, 17(4):499–506, 2003.
- [24] Michael Markl, Alex Frydrychowicz, Sebastian Kozerke, Mike Hope, and Oliver Wieben. 4d flow mri. Journal of Magnetic Resonance Imaging, 36(5):1015–1036, 2012.
- [25] Michael Markl, Alex Frydrychowicz, Sebastian Kozerke, Mike Hope, and Oliver Wieben. 4D flow MRI. Journal of Magnetic Resonance Imaging, 36(5):1015–1036, 2012.
- [26] David Marlevi, Bram Ruijsink, Maximilian Balmus, Desmond Dillon-Murphy, Daniel Fovargue, Kuberan Pushparajah, Cristóbal Bertoglio, Massimiliano Colarieti-Tosti, Matilda Larsson, Pablo Lamata, C. Alberto Figueroa, Reza Razavi, and David A. Nordsletten. Estimation of Cardiovascular Relative Pressure Using Virtual Work-Energy. Scientific Reports, 9(1), December 2019.
- [27] Cristian Montalba, Jesus Urbina, Julio Sotelo, Marcelo E. Andia, Cristian Tejos, Pablo Irarrazaval, Daniel E. Hurtado, Israel Valverde, and Sergio Uribe. Variability of 4D flow parameters when subjected to changes in MRI acquisition parameters using a realistic thoracic aortic phantom. Magnetic resonance in medicine, 79(4):1882–1892, 2018.
- [28] Abbas Nasiraei-Moghaddam, Geoffrey Behrens, Nasser Fatourae, Ramesh Agarwal, Eric T. Choi, and Amir A. Amini. Factors affecting the accuracy of pressure measurements in vascular stenoses from phase-contrast MRI. Magnetic Resonance in Medicine: An Official Journal of the International Society for Magnetic Resonance in Medicine, 52(2):300–309, 2004.

- [29] Elizabeth Nett, Kevin Johnson, Alex Frydrychowicz, Alejandro Muñoz, Eric Schrauben, Christopher Francois, and Oliver Wieben. Four-dimensional phase contrast mri with accelerated dual velocity encoding. Journal of Magnetic Resonance Imaging, 35(6):1462–1471, 2012.
- [30] Fabian Rengier, Michael Delles, Joachim Eichhorn, Yoo-Jin Azad, Hendrik von Tengg-Kobligk, Julia Ley-Zaporozhan, Rüdiger Dillmann, Hans-Ulrich Kauczor, Roland Unterhinninghofen, and Sebastian Ley. Noninvasive 4D pressure difference mapping derived from 4D flow MRI in patients with repaired aortic coarctation: Comparison with young healthy volunteers. The international journal of cardiovascular imaging, 31(4):823–830, 2015.
- [31] Eugénie Riesenkampff, Joao Filipe Fernandes, Sebastian Meier, Leonid Goubergrits, Siegfried Kropf, Stephan Schubert, Felix Berger, Anja Hennemuth, and Titus Kuehne. Pressure fields by flow-sensitive, 4D, velocity-encoded CMR in patients with aortic coarctation. JACC: Cardiovascular Imaging, 7(9):920–926, 2014.
- [32] Y. Saad. Iterative Methods for Sparse Linear Systems. SIAM, Philadelphia, 2nd ed edition, 2003.
- [33] Julio Sotelo, Jesús Urbina, Israel Valverde, Joaquín Mura, Cristián Tejos, Pablo Irarrazaval, Marcelo E. Andia, Daniel E. Hurtado, and Sergio Uribe. Three-dimensional quantification of vorticity and helicity from 3D cine PC-MRI using finite-element interpolations. Magnetic resonance in medicine, 79(1):541–553, 2018.
- [34] Julio Sotelo, Jesus Urbina, Israel Valverde, Cristian Tejos, Pablo Irarrázaval, Marcelo E. Andia, Sergio Uribe, and Daniel E. Hurtado. 3D quantification of wall shear stress and oscillatory shear index using a finite-element method in 3D CINE PC-MRI data of the thoracic aorta. IEEE transactions on medical imaging, 35(6):1475–1487, 2016.
- [35] Abdulrazzaq Sulaiman, Loïc Bousset, Frédéric Taconnet, Jean Michel Serfaty, Hasan Alsaïd, Cherif Attia, Laurent Huet, and Philippe Douek. In vitro non-rigid life-size model of aortic arch aneurysm for endovascular prosthesis assessment. European Journal of Cardio-Thoracic Surgery, 33(1):53–57, 2008.
- [36] H. Švihlová, J. Hron, J. Málek, K. R. Rajagopal, and K. Rajagopal. Determination of pressure data from velocity data with a view toward its application in cardiovascular mechanics. Part 1. Theoretical considerations. International Journal of Engineering Science, 2016.
- [37] Jesús Urbina, Julio A. Sotelo, Daniel Springmüller, Cristian Montalba, Karis Letelier, Cristián Tejos, Pablo Irarrázaval, Marcelo E. Andia, Reza Razavi, and Israel Valverde. Realistic aortic phantom to study hemodynamics using MRI and cardiac catheterization in normal and aortic coarctation conditions. Journal of Magnetic Resonance Imaging, 44(3):683–697, 2016.

- [38] Carole A. Warnes, Roberta G. Williams, Thomas M. Bashore, John S. Child, Heidi M. Connolly, Joseph A. Dearani, Pedro Del Nido, James W. Fasules, Thomas P. Graham, and Ziyad M. Hijazi. ACC/AHA 2008 Guidelines for the Management of Adults With Congenital Heart Disease: Executive Summary: A Report of the American College of Cardiology/American Heart Association Task Force on Practice Guidelines (Writing Committee to Develop Guidelines for the Management of Adults With Congenital Heart Disease) Developed in Collaboration With the American Society of Echocardiography, Heart Rhythm Society, International Society for Adult Congenital Heart Disease, Society for Cardiovascular Angiography and Interventions, and Society of Thoracic Surgeons. Journal of the American College of Cardiology, 52(23):1890–1947, 2008.
- [39] Chih-Yung Wen, An-Shik Yang, Li-Yu Tseng, and Jyh-Wen Chai. Investigation of pulsatile flowfield in healthy thoracic aorta models. Annals of biomedical engineering, 38(2):391–402, 2010.

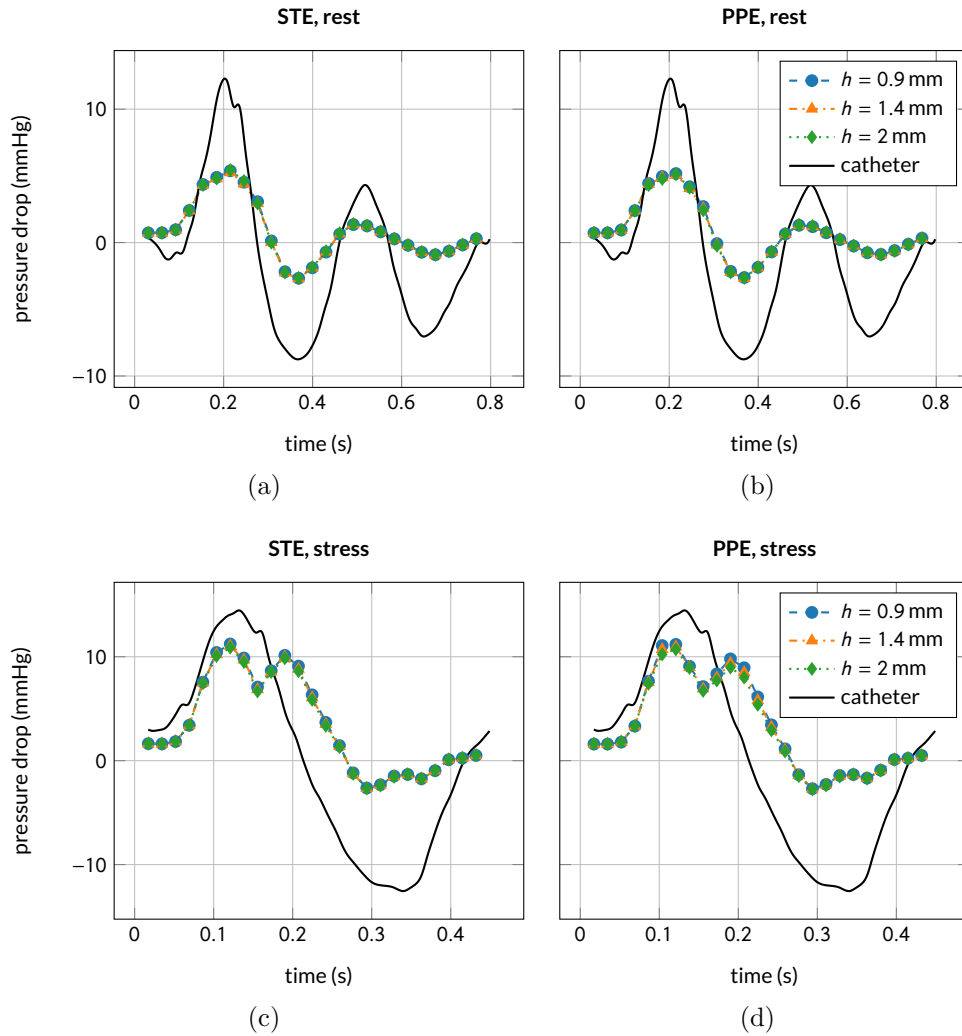


Figure 4: 13 mm AoCo phantom pressure differences obtained with STE (left column) and PPE (right column) under rest (first row) and stress conditions (second row) using voxel sizes of 0.9 mm, 1.4 mm, 2.0 mm compared to ground truth catheter data.

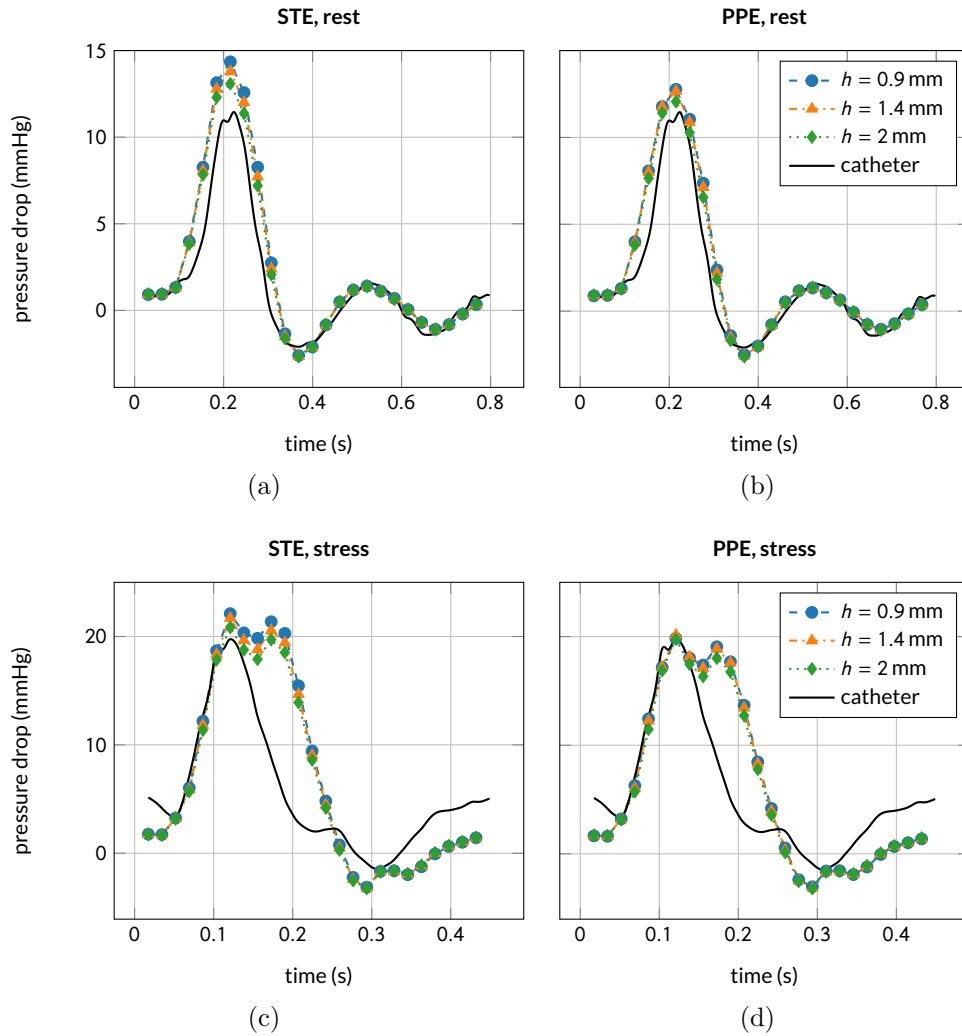


Figure 5: 11 mm AoCo phantom pressure differences obtained with STE (left column) and PPE (right column) under rest (first row) and stress conditions (second row) using voxel sizes of 0.9 mm, 1.4 mm, 2.0 mm compared to ground truth catheter data.

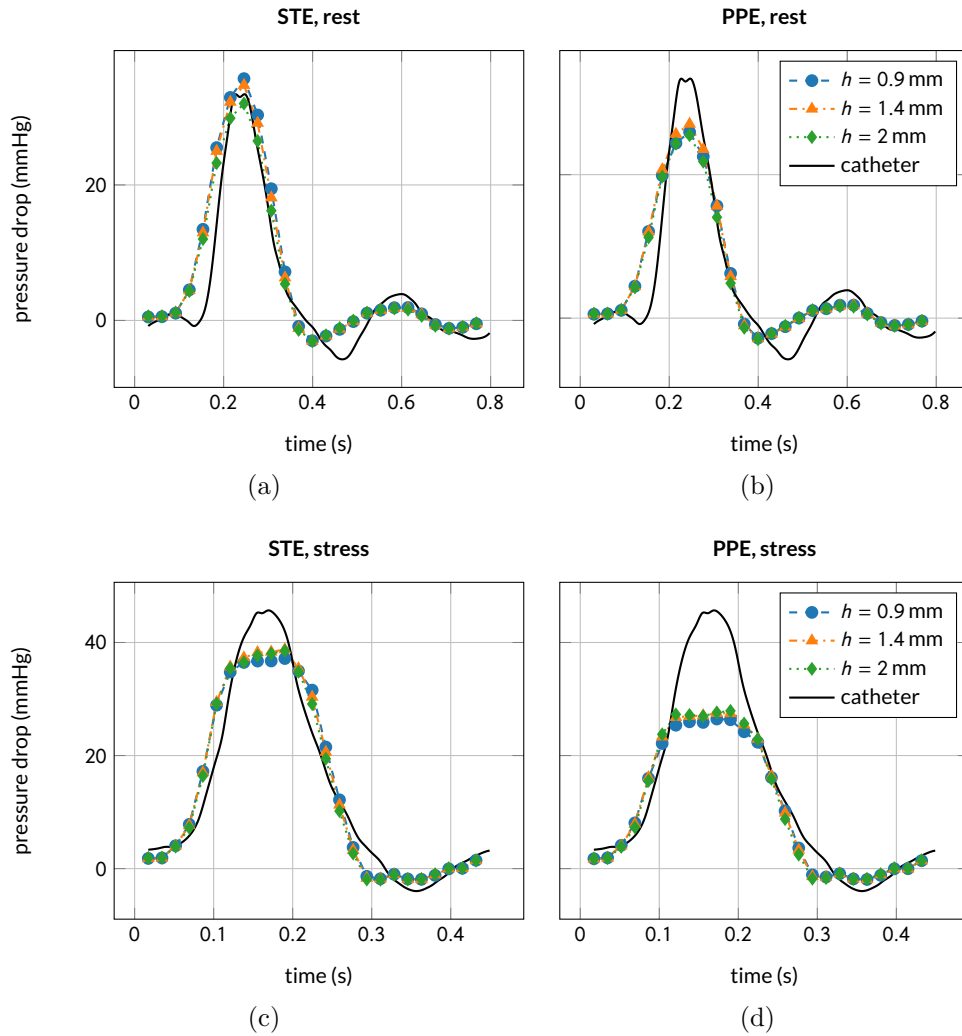


Figure 6: 9 mm AoCo phantom pressure differences obtained with STE (left column) and PPE (right column) under rest (first row) and stress conditions (second row) using voxel sizes of 0.9 mm, 1.4 mm, 2.0 mm compared to ground truth catheter data.

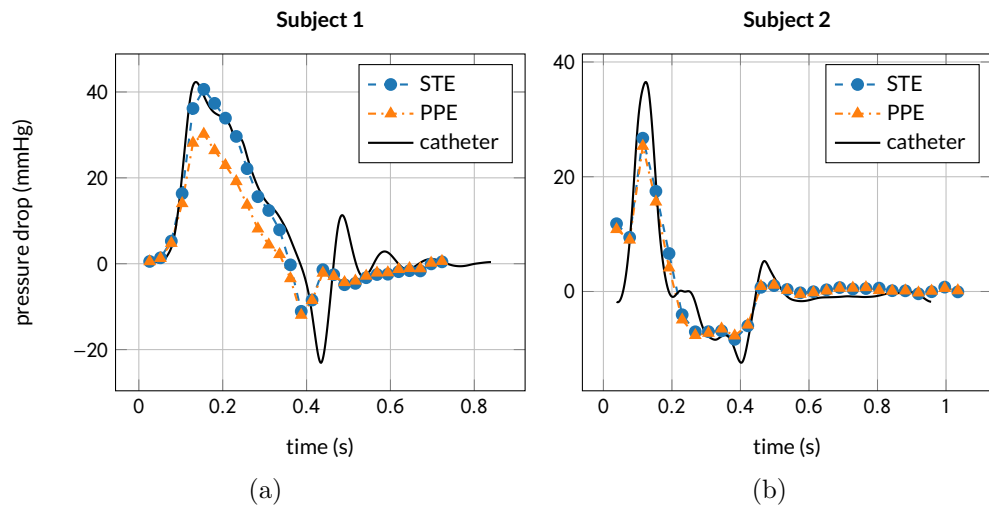


Figure 7: Patient data results, comparison of STE and PPE pressure differences with catheter data